

Effect of net carriers at the interconnection layer in tandem organic solar cells

Li-Jia Chen(陈丽佳), Guo-Xi Niu(牛国玺), Lian-Bin Niu(牛连斌), and Qun-Liang Song(宋群梁)

Citation: Chin. Phys. B, 2022, 31 (**3**): 038802. DOI: 10.1088/1674-1056/ac4485
Journal homepage: http://cpb.iphy.ac.cn; http://iopscience.iop.org/cpb

What follows is a list of articles you may be interested in

Temperature-dependent barrier height inhomogeneities in PTB7:$PC_{71}BM$-based organic solar cells

Brahim Ait Ali, Reda Moubah, Abdelkader Boulezhar, Hassan Lassri
Chin. Phys. B, 2020, 29 (**9**): 098801. DOI: 10.1088/1674-1056/aba5fc

Exploring alkylthiol additives in PBDB-T:ITIC blended active layers for solar cell applications

Xiang Li(李想), Zhiqun He(何志群), Mengjie Sun(孙盟杰), Huimin Zhang(张慧敏), Zebang Guo(郭泽邦), Yajun Xu(许亚军), Han Li(李瀚), Chunjun Liang(梁春军), Xiping Jing(荆西平)
Chin. Phys. B, 2019, 28 (**8**): 088802. DOI: 10.1088/1674-1056/28/8/088802

Electronic states and molecular orientation of ITIC film

Ying-Ying Du(杜莹莹), De-Qu Lin(林德渠), Guang-Hua Chen(陈光华), Xin-Yuan Bai(白新源), Long-Xi Wang(汪隆喜), Rui Wu(吴蕊), Jia-Ou Wang(王嘉鸥), Hai-Jie Qian(钱海杰), Hong-Nian Li(李宏年)
Chin. Phys. B, 2018, 27 (**8**): 088801. DOI: 10.1088/1674-1056/27/8/088801

Self-assembled monolayer modified copper(I) iodide hole transport layer for efficient polymer solar cells

Yuancong Zhong(钟远聪), Qilun Zhang(张琪伦), You Wei(魏优), Qi Li(李琦), Yong Zhang(章勇)
Chin. Phys. B, 2018, 27 (**7**): 078802. DOI: 10.1088/1674-1056/27/7/078802

Efficient ternary organic solar cells with high absorption coefficient DIB-SQ as the third component

Hui-Xin Qi(齐慧欣), Bo-Han Yu(余泊含), Sai Liu(刘赛), Miao Zhang(张苗), Xiao-Ling Ma(马晓玲), Jian Wang(王健), Fu-Jun Zhang(张福俊)
Chin. Phys. B, 2018, 27 (**5**): 058802. DOI: 10.1088/1674-1056/27/5/058802

Effect of net carriers at the interconnection layer in tandem organic solar cells

Li-Jia Chen(陈丽佳)[1,†], Guo-Xi Niu(牛国玺)[2,†], Lian-Bin Niu(牛连斌)[1], and Qun-Liang Song(宋群梁)[2,‡]

[1] *College of Physics and Electronic Engineering, Chongqing Normal University, Chongqing* 401331, *China*
[2] *Institute for Clean Energy & Advanced Materials, School of Materials and Energy, Southwest University, Chongqing* 400715, *China*

(Received 28 September 2021; revised manuscript received 30 November 2021; accepted manuscript online 18 December 2021)

Tandem cell with structure of indium tin oxide (ITO)/molybdenum oxide (MoO_3)/fullerene (C60)/copper phthalocyanine (CuPc)/C60/tris-8-hydroxy-quinolinato aluminum (Alq_3)/Al was fabricated to study the effect of net carriers at the interconnection layer. The open circuit voltage and short circuit current were found to be 1.15 V and 0.56 mA/cm^2, respectively. Almost the same performance (1.05 V, 0.58 mA/cm^2) of tandem cell with additional recombination layer (ITO/MoO_3/C60/Alq_3/Al/Ag/MoO_3/CuPc/C60/Alq_3/Al) demonstrates that the carrier balance is more crucial than carrier recombination. The net holes at the interconnection layer caused by more carrier generation from the back cell on one hand would enhance the recombination with electrons from the front cell and on the other hand would quench the excitons produced in CuPc of the back cell.

Keywords: tandem organic solar cells, interconnection layer, carrier balance, carrier-exciton interaction

PACS: 88.40.jr, 72.20.Jv, 73.40.–c, 85.30.De **DOI:** 10.1088/1674-1056/ac4485

1. Introduction

Solar energy is one of the best available alternatives to reduce the usage of and finally replace fossil fuels.[1,2] Though the efficiency and lifetime are still low, in the past decade, organic solar cells (OPVs) and perovskite solar cells (PSCs) have emerged and are promising alternatives to inorganic solar cells because of their low processing cost, ease of processibility, roll-to-roll processiblity for large area devices and mechanical flexibility.[3–7] Various strategies have been applied to enhance the efficiency of OPVs including controlling morphology,[8] utilizing low band gap materials,[9] and designing novel structures.[10] One reason for the low efficiency is the narrow absorption spectrum of OPVs,[11,12] and another reason is the relative thin organic layer used in OPVs due to the short exciton diffusion length.[2,13] Tandem structure can resolve these problems by using different organic materials to cover a broader absorption spectrum and thicker active layer to absorb more light in the cells.[12,14,15]

Besides the more light absorption, carrier balance and efficient carrier recombination at the interconnection are also very important for high performance tandem OPVs.[16] Unless the carrier balance is met, net carriers would appear at the interconnection to reduce the serial voltage output or even to quench excitons generated by light absorption.[17] Similar voltage loss and exciton quenching would occur if the recombination at the interconnection is not efficient even if the carrier balance is meet.[14,18] Efforts have been devoted to achieve the carrier balance through material choosing[16] and thickness optimization,[14,19] to realize efficient recombination by using nano-metal cluster,[20,21] a p–n junction,[14,16] or a doped functional material as interconnection layer.[22,23] Recently, we found that the free carrier can be generated through interfacial exciton recombination[24] or electron–exciton interaction.[25] Since carrier balance and efficient recombination at the interconnection layer are not always met in tandem devices, it is necessary to study effect of net carriers at the interconnection layer.

In this work, a serial tandem device with structure of indium tin oxide (ITO)/molybdenum oxide (MoO_3)/fullerene (C60)/copper phthalocyanine (CuPc)/C60/tris-8-hydroxy-quinolinato aluminum (Alq_3)/Al was fabricated to study the effect of net carriers at the first C60–CuPc interface. It is found that carrier balance is more important than efficient carrier recombination at the interconnection layer when the photocurrent is small. The net carriers piled up at the interconnection layer of a tandem cell would reduce the voltage and photocurrent output. Due to these net carriers, both enhancement and reduction of external quantum efficiency (EQE) are found in the same device under light bias.

2. Experimental details

The structure of the tandem cells studied is depicted in the inset of Fig. 2. ITO coated glass having a sheet resistance about 15 Ω/square was cleaned by detergent Decon 90 before film deposition. The tandem OPV was fabricated in a high vacuum chamber with a base pressure of 5.0×10^{-6} Pa. The deposition rate of organic materials was kept at $\sim$ 0.04 nm/s and monitored by a calibrated quartz oscillator. A 100 nm

†These authors contributed equally to this work.
‡Corresponding author. E-mail: qlsong@swu.edu.com

© 2022 Chinese Physical Society and IOP Publishing Ltd

thick Al electrode was deposited on top of the organic active layers through a shadow mask that defines an active area of 9 mm^2. The device was characterized in a nitrogen-purged glove box, which is connected to the device fabrication system. The EQE was calculated from the I_{sc} measured by SR830 (Stanford Research Systems Inc.) lock-in amplifier. The white light bias is produced from a halogen tungsten lamp. The current density–voltage (J–V) characteristics were conducted by Keithley 2400 (Keithley Instruments Inc.) under air mass 1.5 global (AM 1.5G) illumination of 100 mW/cm^2 (Newport solar simulator model 94043A).

3. Results and discussion

The structure of organic solar cells (OSCs) is shown in Fig. 1. The structures for subcells A and B are ITO/MoO_3 (5 nm)/C60 (40 nm)/Alq_3 (5 nm)/Al (100 nm), ITO/CuPc (25 nm)/C60 (50 nm)/Alq_3 (5 nm)/Al(100 nm), respectively. The structures of tandem devices C and D are ITO/MoO_3 (5 nm)/C60 (40 nm)/Alq_3 (2 nm)/Al (1 nm)/Ag (1 nm)/MoO_3 (3 nm)/CuPc (20 nm)/C60 (50 nm)/Alq_3 (5 nm)/Al and ITO/MoO_3 (5 nm)/C60 (40 nm)/CuPc (25 nm)/C60 (50 nm)/Alq_3 (5 nm)/Al (100 nm), respectively.

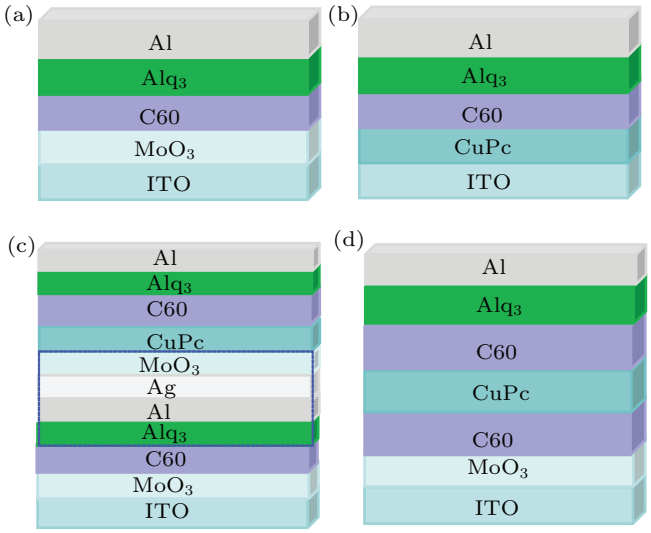


Fig. 1. The structures of the four devices.

Figure 1 shows the J–V curves of the best four devices, in which devices A and B are the subcells used in tandem devices C and D. The open circuit voltage (V_{oc}) and short circuit current (I_{sc}) are 1.01 V, 1.33 mA/cm^2 and 0.45 V, 3.75 mA/cm^2 for devices A and B, respectively, consistent with the reported values.[26,27] A statistical analysis was performed on 10 OPVs for each device, and the corresponding results are summarized in Fig. 3. It reacts the same trend as suggested by the comparison of best devices. The best performance of four devices can be read out from Table 1 that the V_{oc} and I_{sc} are 1.05 V, 0.58 mA/cm^2 and 1.15 V, 0.56 mA/cm^2, respectively, for tandem devices C and D. The performance difference between the two tandem devices is quite small and the only difference between C and D is the recombination interlayer (Alq_3 (2 nm)/Al (1 nm)/Ag (1 nm)/MoO_3 (3 nm)) used in device C. The possible reason is the small photocurrent obtained in these two devices and thus high efficient recombination interconnection layer is not necessary.

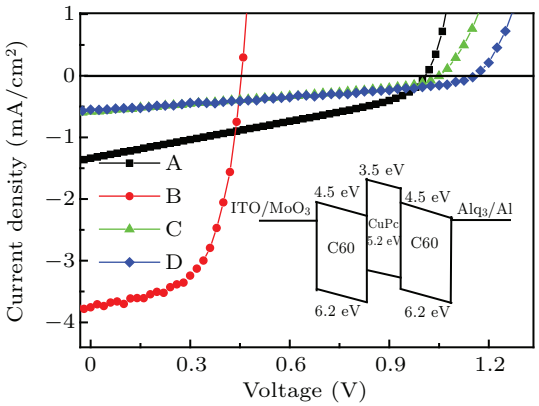


Fig. 2. The J–V characterization of devices A, B, C, and D.

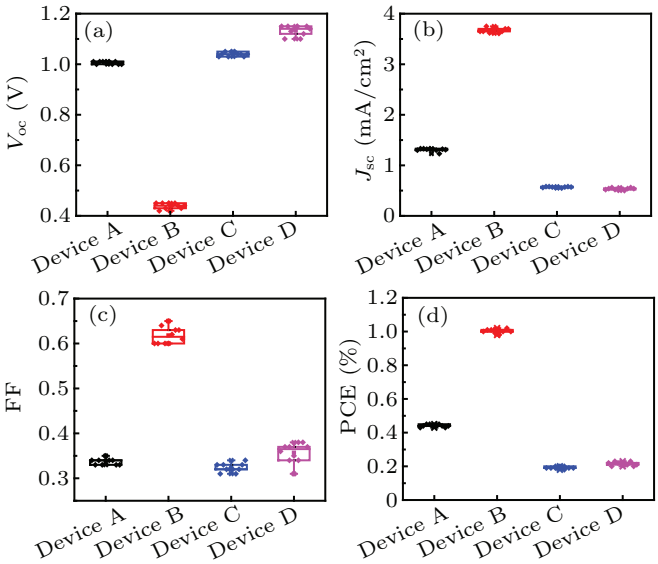


Fig. 3. Statistical analysis of the photovoltaic performance from 10 OPVs for devices A, B, C, and D.

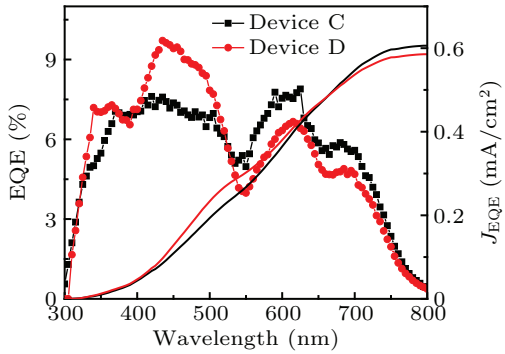


Fig. 4. EQE spectrum and the integrated current density for devices C and D.

The optical distribution and light absorption in devices C and D are quite similar. The external quantum efficiency (EQE) spectrum and its corresponding integral current density

(J_{EQE}) for devices C and D are observed in Fig. 4. The integral currents are 0.60 mA/cm^2 (device C) and 0.58 mA/cm^2 (device D), which are consistent with the J_{sc} results extracted from the J–V characteristics as Table 1.

Table 1. Best parameters of devices A, B, C and D.

Device	V_{oc} (V)	J_{sc} (mA/cm^2)	FF	P_{max} (mW/cm^2)
A	1.01	1.33	0.34	0.45
B	0.45	3.75	0.60	1.02
C	1.05	0.58	0.33	0.20
D	1.15	0.56	0.36	0.23

The optical calculation is subject to Bruggeman's effective medium approximation. The calculation program from the website (numpy.scipy.org) is an open source program which is based on Python language. The optical constant and thickness of materials are compiled into the document, which is recognized by the software as the input document of the model. The material and thickness of each layer were input the corresponding documents to complete the data establishment of the device model, by using the refractive index n and extinction coefficient k of substrate ITO from Ref. [28], of MoO_3 from Ref. [29], of CuPc from Ref. [30], of C60 from Ref. [31] and Alq_3 from Ref. [32]. Optical calculation by transfer matrix[33] shows that the small photocurrent is caused by the unbalanced carriers from the subcells. As shown in Fig. 5, the light with wavelength shorter than 550 nm is mainly absorbed by C60 while light with wavelength longer than 550 nm is mainly absorbed by CuPc.[34] The much larger number of photons absorbed by the back cell (indeed, the I_{sc} of device B is much larger than that of device A) indicates that net carriers (holes) might exist at the interconnection of the two subcells. The voltage reduction ($\sim$ 0.4 V) caused by these holes at the interconnection is the reason for the smaller voltage compared to the sum of the two subcells ($\sim$ 1.5 V).

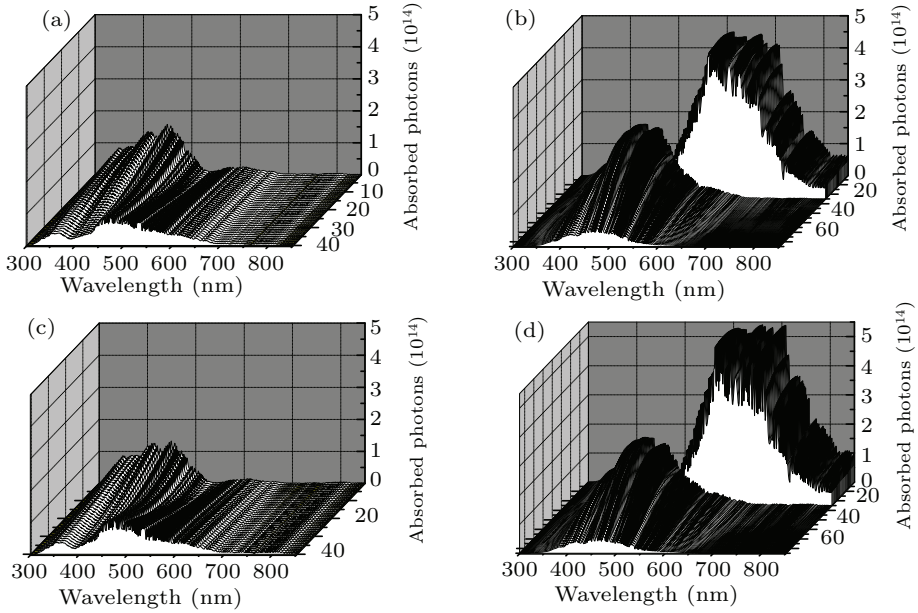


Fig. 5. The calculated light absorption distribution in devices C ((a), (b)) and D ((c), (d)) (front cell (a), (c) and back cell (b), (d)) based on transfer matrix. The input of the light illumination is 100 mW/cm^2 AM 1.5G sunlight.

Figure 6 shows the EQE of devices C and D with and without light bias. Both EQEs and their corresponding phases measurements (as shown in Figs. 6(c) and 6(d)) are similar. The tandem cells show photoresponse in the whole wavelength range of 300–800 nm, which means both C60 and CuPc contribute to the photocurrent. However, the contribution from CuPc (550–800 nm) decreases under light bias, and the stronger the light bias is, the more decrease can be observed. Interestingly, the response in the UV range which can be assigned to the response of C60 is enhanced under light bias. The integration of EQE under 100% light bias by AM1.5G spectrum is equal to the I_{sc} measured. The large phase shift under light bias is an indicator of displacement current in the 550–800 nm range.[22] Thus, it can be concluded that the photocurrent mainly comes from the contribution of C60. The analysis of the physical processes happened in the tandem devices is much helpful for understanding the phenomena we observed. Due to the special structure chosen in this study, the photons absorbed by the back cell are much more than those absorbed by the front device, as shown in Fig. 5. Most excitons produced in the front cell are separated at the MoO_3–C60 interface and most excitons generated in the back cell are dissociated at the second CuPc–C60 interface, which are similar to the subcells A and B, respectively. Electrons left in the front cell would recombine with holes coming from the back cell to make the tandem cell work properly. The recombination occurs at the interconnection (the first C60–CuPc interface, inset of Fig. 1) between the front cell and the back cell, where ex-

citons can also be dissociated, especially for device D without recombination layer. Holes and electrons would be collected by ITO and Al electrodes, respectively, as the *J*–*V* measurements show, and thus exciton dissociation at the first C60–CuPc interface would cause reverse flowing of carriers and generating displacement current as observed in Fig. 6. Both electrons left in the first C60 layer and holes generated from exciton dissociation at the second CuPc–C60 interface pile up at the first C60–CuPc interface with the help of built-in electric field in the device. The large energy barriers encountered by these carriers boost their recombination and at the same time these holes and electrons quench excitons in CuPc and in the first C60 layer, respectively. As shown in Fig. 5, the back cells absorb more illumination than the subcells, which results to the more exciton at the back cells. At the free carriers at CuPc–C60 interface is more than at the MoO_3–C60 interface, and the left carriers were combination. However, the left carriers can not be balanced. The net carriers would appear at the interconnection to reduce the serial voltage output or even to quench excitons generated by light absorption. The fourth but not last process happens at the first C60–CuPc interface is the carrier–exciton interaction to help the carriers to overcome the energy barrier.[25] In brief, four processes coexist at the interconnection between the front and back cells: exciton dissociation, carrier recombination, exciton quench, and carrier–exciton interaction. Unless the exciton–exciton interaction is considered, the exciton dissociation will not be affected by light bias, which is also the case for subcells. But other three processes can be modulated by light bias, resulting in the modulation of apparent EQE. Indeed light bias changes the apparent EQE of tandem device (as shown in Fig. 6) but has no effect on subcells (not shown here).

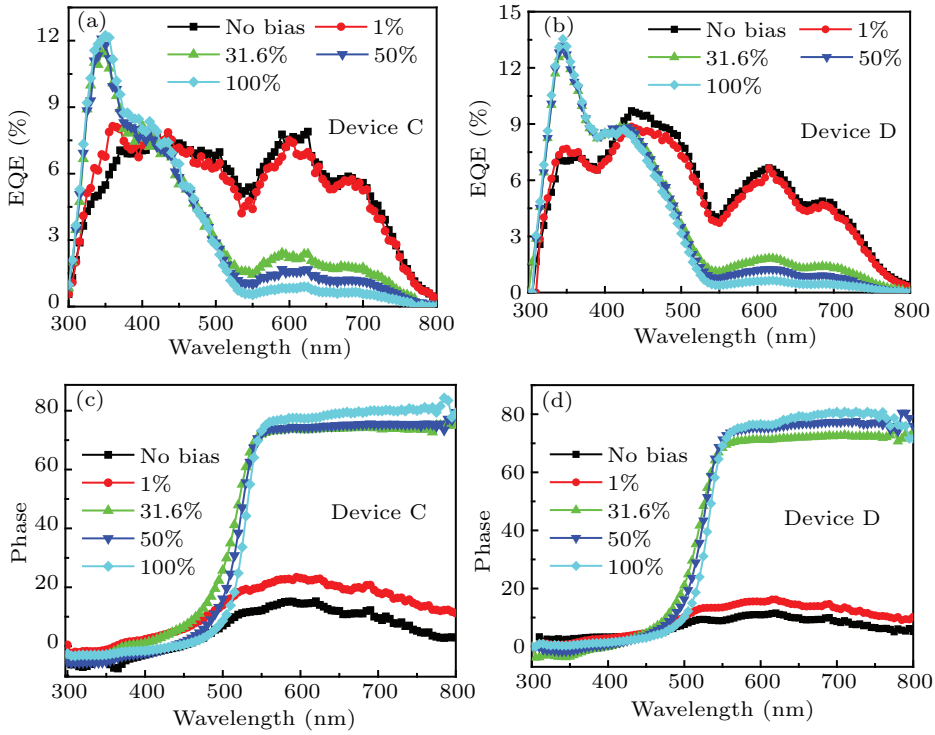


Fig. 6. The EQE of devices (a) C and (b) D with and without white light bias. The intensity of the light bias is changed by neutral density filter and its value is shown in the inset. The phase information of the EQE measurements of devices C and D is shown in (c) and (d), respectively.

To further understand the effect of net carriers at the interconnection, C60 and CuPc are selectively excited by using 450 nm and 620 nm band pass filter, as shown in Fig. 7(a). Figure 7(b) shows the EQE measurements under light bias compared with the one without light bias. Similar to the white light bias, both blue and red light biases modulate the apparent EQE with increase and decrease in range of 300–400 nm and 500–800 nm, respectively. The modulation is more prominent by selective exciting CuPc with red light bias. Red light bias selectively excites CuPc to produce excitons for dissociation at the second CuPc–C60 interface. Electrons are collected by the Al electrode while net holes are piled up at the first CuPc–C60 interface. These holes are waiting there to quench the excitons in CuPc produced by chopped monochromatic light (500–800 nm), decreasing the apparent EQE in this range. When the chopped monochromatic light (300–400 nm) excites C60, these holes would accelerate the recombination with the electrons coming from the first C60, increasing the apparent EQE accordingly. When changed to blue light bias which is stronger than red light bias for our study, it selectively excites both C60 layers to produce excitons for dissociation at MoO_3–C60 and the second CuPc–C60 interfaces. The number of excitons in the second C60 layer is larger than that in the first C60 layer, as shown in Fig. 5. Thus most of holes

(net carrier) in CuPc would recombine with the electrons (net carrier) from the first C60 layer. Similar processes would happen like red light bias since the left holes are piled up at the first CuPc–C60 interface. Due to the fewer holes (net carrier) at the first CuPc–C60 interface, the apparent EQE decrease in 500–800 nm and increase in 300–400 nm are less prominent than the case of red light bias.

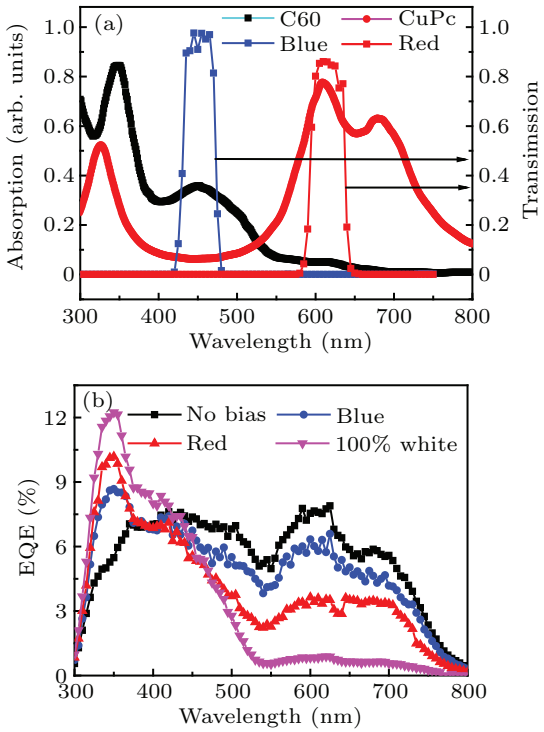


Fig. 7. (a) The absorption spectra of CuPc and C60; the transmission of blue and red band pass filters. The blue and red light biases used in this study are realized by put a band pass filter before a white light. (b) Apparent EQE modulation by light biases.

4. Conclusion

By intentionally choosing the device configuration, the carrier balance is broken to accumulate net carriers at the interconnection layer of a tandem cell. By carefully studying the effect of these net carriers by using light bias, the importance of carrier balance in tandem OPVs is identified. Exciton dissociation, carrier recombination, exciton quenching, and carrier–exciton interaction coexist at the interconnection of a tandem device. By using light bias technique, these processes are modulated, reflecting in the apparent EQE variation.

Acknowledgement

This work was supported by the National Natural Science Foundation of China (Grant Nos. 11774293, 1207432, and 61874016).

References

[1] Sampaio P G V, González M O A, Oliveira F P, Cunha J V P, Pereira, J P P, Ferreira H R and Oprime P C 2020 *Int. J. Energy Res.* **44** 9912
[2] Xue J R, Uchida B P and Forrest S R 2005 *Adv. Mater.* **17** 66
[3] Ali B A, Moubah R, Boulezhar A and Lassri H 2020 *Chin. Phys. B* **29** 098801
[4] Park J W, Takaloo A V, Kim S H, Son K R, Kang D Y, Kang S K, Lee C B, Choi H, Shim J W and Kim T G 2021 *J. Power Sources* **489** 229507
[5] Zhang L, Liu W N, Wang Y Z, Liu Q M, Li J S, Li Y L and He D Y 2021 *Chin. Phys. B* **30** 104207
[6] Li F, Duan W, Pomaska M, Köhler M, Ding K, Pu Y, Aeberhard U and Rau U 2021 *Chin. Phys. Lett.* **38** 036301
[7] Qu Z, Ma F, Zhao Y, Chu X, Yu S and You J 2021 *Chin. Phys. Lett.* **38** 107801
[8] Munshi J, Chien T, Chen W and Balasubramanian G 2020 *Soft Matter* **16** 6743
[9] Cheng P and Yang Y 2020 *Acc. Chem. Res.* **53** 1218
[10] Khlaifia D, Massuyeau F, Ewels C P, Duvail J L, Faulques E and Alimi K 2017 *Chemisty Select* **2** 10082
[11] Lassiter B E, Zimmerman, J D, Panda A, Xiao X and Forrest S R 2012 *App. Phys. Lett.* **101** 063303
[12] Dennler G, Prall H J, Koeppe R, Egginge M, Autengruber R and Sariciftci N S 2006 *App. Phys. Lett.* **89** 073502
[13] Peumans P, Yakimov A and Forrest S R 2003 *J. App. Phys.* **93** 3693
[14] Macko J A, Lunt R R, Osedach T P, Brown P R, Barr M C, Gleason K K and Bulovic V 2012 *Phys. Chem. Chem. Phys.* **14** 14548
[15] Ameri T, Dennler G, Lungenschmied C and Brabec C J 2009 *Energy Environ. Sci.* **2** 347
[16] Yu B, Zhu F, Wang H B, Li G and Yan D H 2008 *J. Appl. Phy.* **104** 114503
[17] Timmreck R, Olthof S, Leo, K and Riede M K 2010 *J. Appl. Phys.* **108** 033108
[18] Seo J H, Kim D H, Kwon S H, Song M, Choi M S, Ryu S Y, Lee H W, Park Y C, Kwon J D, Nam K S, Jeong Y, Kang J W and Kim C S 2012 *Adv. Mater.* **24** 4523
[19] Gilot J, Wienk M M and Janssen R A J 2010 *Adv. Mater.* **22** E67
[20] Steirer K X, MacDonald G A, Olthof S, Gantz J, Ratcliff E L, Kahn A and Armstrong N R 2013 *J. Phys. Chem. C* **117** 22331
[21] Yakimov A and Forrest S R 2020 *Appl. Phys. Lett.* **80** 1667
[22] Ishiyama N, Kubo M, Kaji T and Hiramoto M 2012 *Appl. Phys. Lett.* **101** 233303
[23] Ishiyama N, Kubo M, Kaji T and Hiramoto M 2013 *Org. Electron.* **14** 1793
[24] Song Q L, Yang H B, Gan Y, Gong C and Li C M 2010 *J. Am. Chem. Soc.* **132** 4554
[25] Chen L, Zhang Q, Lei Y, Zhu F, Wu B, Zhang T, Niu G, Xiong Z and Song Q 2013 *Phys. Chem. Chem. Phys.* **15** 16891
[26] Song Q L, Li F Y, Yang H, Wu H R, Wang X Z, Zhou W, Zhao J M, Ding X M, Huang C H and Hou X Y 2005 *Chem. Phys. Lett.* **416** 42
[27] Zhang M L, Irfan, Ding H J, Gao Y L and Tang C W 2010 *Appl. Phys. Lett.* **96** 183301
[28] Hoppe H, Sariciftci N S and Meissner D 2002 *Mol. Cryst. Liq. Cryst.* **385** 113
[29] Abdellaou A, Donnadieu G L A, Bath A and Bouchikhi B 1997 *Thin Solid Films* **304** 39
[30] Elmas D N and Çapan I 2019 *Indian J. Phys.* **94** 1061
[31] Pettersson, L A A, Roman L S and Inganäs O 1999 *J. Appl. Phys.* **86** 487
[32] Xie W, Zhao Y, Hou J and Liu S 2003 *Jpn. J. App. Phys.* **42** 1466
[33] Song Q L , Yang H, Wu H R and Li F Y 2006 *J. Lumin.* **119** 142
[34] Zhao X, Li Z, Zhu T, Mi B, Gao Z and Huang W 2013 *J. Phys. D App. Phys.* **46** 195105